Final Report on Radiative Effects of Aerosols

Principal Investigator: Francisco P.J.Valero
Atmospheric Research Laboratory
Scripps Institution of Oceanography
University of California, San Diego
9500 Gilman Drive
La Jolla, California 92093-0242
Ph: 619-534-8099

The paper "Vertical Profiles, Aerosol Microphysics and Optical Closure during ASTEX: Measured and Modeled Column Optical Properties", Clarke et al, describes the work done during the period of this grant. It can be summarized as follows:

During the Atlantic Stratocumulus Transition Experiment (ASTEX) in June 1992, two descents in cloud-free regions allowed comparison of the change in aerosol optical depth as determined by an onboard total-direct-diffuse radiometer (TDDR) to the change calculated from measured size-resolved aerosol microphysics and chemistry. Both profiles included pollution haze layer from Europe but the second also included the effect of a Saharan dust layer above the haze. The separate contributions of supermicrometer (coarse) and submicrometer (fine) aerosol were determined and thermal analysis of the pollution haze indicated that the fine aerosol was composed primarily of a sulfate/water mixture with a refractory soot-like core. The soot core increased the calculated extinction by about 10% in the most polluted drier layer relative to a pure sulfate aerosol but had significantly less effect at higher humidities. A 3 km descent through a boundary layer airmass dominated by pollutant aerosol with relative humidities (RH) 10-77% yielded a close agreement between the measured and calculated aerosol optical depths (550nm) of 0.160 (+/- 0.07) and 0.157 (+/- 0.034) respectively. During descent the aerosol mass scattering coefficient per unit sulfate mass (inferred) varied from about 5 to 16m^2g^{-1} and primarily dependent upon ambient RH. However, the total scattering coefficient per total fine mass was far less variable at about 4+/- 0.7m^2g^{-1}. A subsequent descent through a Saharan dust layer located above the pollution aerosol layer revealed that both layers contributed similarly to aerosol optical depth. The scattering per unit mass of the coarse aged dust was estimated at 1.1 +/- 0.2m^2g^{-1}. The large difference (50%) in measured and calculated optical depth for the dust layer exceeded estimated measurement

uncertainty (12%). This is attributed to inadequate data on the spatial variability of the aerosol field within the descent region, a critical factor in any validation of this type. Both cases demonstrate that surface measurements may be a poor indicator of the characteristics and concentration of the aerosol column.

The optical properties of Arctic Haze were studied using a total-direct-diffuse radiometer as part of the Arctic Gas and Aerosol Sampling Project, part III (AGASP III). The radiometer was installed on the NOAA WP-3D research aircraft and measured solar downwelling irradiance in seven narrow-band channels in the visible and near-infra-red. Haze optical depths had maximum values near 0.1 in the mid-visible for AGASP flights 310 and 311. An inferred particle size spectrum from flight 311 extinction measurements showed two dominant modes near 0.1 and 0.8 μm. A method of retrieving the angular dependence of scattered radiation is presented and suggests the presence of thin cirrus.

The radiative effects of the smoke from the Kuwait oil fires were assessed by measuring downwelling and upwelling solar air flux, as well as spectral solar extinction beneath, above and within the smoke plume. Radiative flux divergence measurements were made to determine smoke-induced heating and cooling rates. Seven radiation flight missions were undertaken between May 16 and June 2, 1991, to characterize the plume between the source region in Kuwait and approximately 200 km south, near Manama, Bahrain. We present results from one flight representative of conditions of the composite plume. On May 18, 1991, in a homogeneous, well-mixed region of smoke approximately 100 km downstream of the fires, visible optical depths as high as 2 were measured, at which time transmission to the surface was 8%, while 78% of the solar radiation was absorbed by the smoke. The calculated instantaneous heating rate inside the plume reached 24K/d. While these effects are probably typical of those regions in the Persian Gulf area directly covered by the smoke, there is no evidence to suggest significant climatic effects in other regions.

JOURNAL OF GEOPHYSICAL RESEARCH, VOL. 101, NO. D2, PAGES 4443–4453, FEBRUARY 20, 1996

Vertical profiles, aerosol microphysics, and optical closure during the Atlantic Stratocumulus Transition Experiment: Measured and modeled column optical properties

A.D. Clarke and J. N. Porter

School of Ocean and Earth Science and Technology, University of Hawaii, Honolulu

F.P.J. Valero

California Space Institute, University of California, San Diego, La Jolla

P. Pilewskie

NASA, Ames Research Center, Moffett Field, California

Abstract. During the Atlantic Stratocumulus Transition Experiment (ASTEX) in June 1992, two descents in cloud-free regions allowed comparison of the change in aerosol optical depth as determined by an onboard total-direct-diffuse radiometer (TDDR) to the change calculated from measured size-resolved aerosol microphysics and chemistry. Both profiles included a pollution haze layer from Europe, but the second also included the effect of a Saharan dust layer above the haze. The separate contributions of supermicrometer (coarse) and submicrometer (fine) aerosol were determined, and thermal analysis of the pollution haze indicated that the fine aerosol was composed primarily of a sulfate/water mixture with a refractory sootlike core. The soot core increased the calculated extinction by about 10% in the most polluted drier layer relative to a pure sulfate aerosol but had significantly less effect at higher humidities. A 3-km descent through a boundary layer air mass dominated by pollutant aerosol with relative humidities (RH) 10-77% yielded a close agreement between the measured and calculated aerosol optical depths (550 nm) of 0.160 (±0.07) and 0.157 (±0.034), respectively. During descent the aerosol mass scattering coefficient per unit sulfate mass (inferred) varied from about 5 to 16 $m^2 g^{-1}$ and was primarily dependent upon ambient RH. However, the total scattering coefficient per total fine mass was far less variable at about 4 ±0.7 $m^2 g^{-1}$. A subsequent descent through a Saharan dust layer located above the pollution aerosol layer revealed that both layers contributed similarly to aerosol optical depth. The scattering per unit mass of the coarse aged dust was estimated at 1.1 ± 0.2 $m^2 g^{-1}$. The large difference (50%) in measured and calculated optical depth for the dust layer exceeded estimated measurement uncertainty (12%). This is attributed to inadequate data on the spatial variability of the aerosol field within the descent region, a critical factor in any validation of this type. Both cases demonstrate that surface measurements may be a poor indicator of the characteristics and concentration of the aerosol column.

Introduction

Issues involving the physical, chemical, and optical properties of tropospheric aerosol are presently responsible for several major research programs and many individual investigations. One area of current concern includes the influence of aerosol optical properties on radiative transfer in the atmosphere due to their direct interaction with radiation [*Charlson et al.*, 1992] or through the indirect influence as cloud condensation nuclei, CCN, upon cloud properties [*Charlson et al.*, 1987; *Twomey*, 1977]. Included are issues such as possible climate forcing by sulfate aerosol [*Charlson et al.*, 1992], the significance of sulfate and soot emissions from both anthropogenic and biomass burning [*Penner et al.*, 1993], the influence of dimethylsulfide (DMS) emissions upon aerosol and CCN formation [*Ayers and Gras*, 1991] and the radiative effects of both volcanic and extensive dust plumes advected aloft [*d'Almeida*, 1987; *Carlson and Caverly*, 1977]. Motivation for many of these studies originates from general concern over the radiative influence of aerosol including the potential for radiative forcing of global climate [*Penner et al.*, 1993; *Kiehl and Briegleb*, 1993] and from the practical need for the reliable interpretation of satellite-derived radiances (eg. advanced very high resolution radiometer (AVHRR), Sea-viewing Wide Field-of-view Sensor, (SeaWiFS), particularly for marine environments [*Hooker and Firestone*, 1992]. However, the interpretation of satellite-retrieved radiances requires some assumptions about an appropriate global aerosol model. A major weak point in the development of an appropriate model is the dearth of measurements of key aerosol

Paper number 95JD03140.
0148-0227/96/95JD-03140 $05.00

properties over much of the globe [*Penner et al*, 1993]. It is also recognized that measurements are particularly sparse for aerosol properties in the vertical and their relationship of aerosol aloft to the more commonly studied surface aerosol. Because of the suitability of marine regions for the satellite retrieval of aerosol properties, an improved characterization of marine aerosol is of particular interest.

The remote marine aerosol is a dynamic reservoir of particles originating from diverse marine, continental and in situ sources. It is well known that sea salt [*Woodcock, 1953*], dust [*Prospero and Carlson*, 1972], sulfate and nitrate [*Savoie and Prospero*, 1982], methane sulfonate (MSA) [*Saltzman et al.*, 1986] and soot [*Clarke*, 1989] can be important contributors to marine aerosol mass and composition. The marine aerosol mass distribution is predominantly bimodal with a coarse mode dominated by sea salt and/or dust and a fine mode usually dominated by sulfate [*Clarke et al.*, 1987 a,b; *Savoie and Prospero*, 1982]. Moreover, the marked decrease in sea-salt aerosol mass (dominated by the largest salt particles) with altitude [*Woodcock*, 1953] means that the relative importance of fine sulfate aerosol can increase with altitude. Soot is usually only a small contributor to the fine mode but in some regions it can have a significant effect on aerosol optical properties due to its light-absorbing properties (e.g., pollution, biomass burning [*Clarke*, 1988]). Other common species can include nitrates but these are usually associated with the surface area peak of the coarse sea-salt mode [*Savoie and Prospero*, 1982], while MSA (an oxidation product of DMS) appears to contribute in a variable but small way to both modes [*Huebert et al.*, 1993]. Other constituents (e.g., organics) may also be present but are poorly characterized in marine regions. It is this aerosol composition that determines its refractive index as well as its growth due to the uptake of water in response to increasing RH [*Tang and Munkelwitz*, 1977]. Hence the size distribution, composition (including water), and state of mixing (internal/external) of the aerosol components comprise the essential information for modeling their radiative properties, important not only for climate modeling but also for accurate determination of global aerosol optical depths from present and future satellites (e.g., AVHRR and SeaWiFS). Here we will use measured size-resolved aerosol physicochemistry during vertical profiles over the Atlantic to model aerosol optical extinction for comparison to directly measured extinction profiles. The comparison will be used to provide an assessment of "closure" [*Penner et al.*, 1993] between measured and modeled quantities and to reveal the practical sources of uncertainty in this type of intercomparison.

Instrumentation

Interest in the above issues prompted our participation in the Atlantic Stratocumulus Transition Experiment (ASTEX) as part of the Marine Aerosol and Gas Experiment (MAGE) aboard the Electra [*Huebert et al.*, this issue]. Here we report on two cases where aerosol vertical profiles were obtained in clear air and with the absence of high-level clouds. Our aerosol instrumentation employed a laser optical particle counter (OPC) (custom LAS-X, Particle Measurement Systems, Boulder, Colorado), to size particles with diameters (Dp) of 0.15-7.5 μm. This was operated at low relative humidity (RH) at three temperatures (40°, 150°, 300°C) in order to characterize aerosol volatility related to its composition [*Clarke*, 1991]. Field calibrations include latex spheres to test stability while laboratory calibrations included calibration curves generated with sulfuric acid, ammonium sulfate, ammonium bisulfate and sea-salt. Calibrations based upon compositions inferred from thermal volatility were used for sizing the dry aerosol with appropriate diameter shifts applied in order to simulate the aerosol at higher humidities [*Clarke*, 1991]. Size distributions of smaller nuclei ($0.02<Dp<0.6$ μm) were also obtained at these temperatures from a differential mobility analyzer (DMA). Both were operated below about 20% RH in order minimize size variations in response to water uptake and to allow inference of chemical composition. Condensation nuclei (CN) counters also provided a continuous measurements of the aerosol number concentration with diameters above 3nm.

An aethaelometer (Magee Scientific) provided aerosol light absorption measurements for the assessment of combustion derived black carbon (BC) concentrations and the related aerosol absorption coefficient, B_{ab} (see below). We note that the aethaelometer is reported to measure BC based upon a calibration derived from thermally evolved CO_2 [*Gundel et al.*, 1984] and the presumption that BC is the only significant absorber. However, the actual measurement is one of attenuation of light through a filter due to aerosol absorption. Hence absorbers other than BC can contribute to the attenuation. Nevertheless, we have used the BC calibration [*Gundel et al.*, 1984] and a reasonable specific absorption (absorption per unit mass) for soot in the observed size range (see Figure 2) of 10 $m^2 g^{-1}$ to convert the inferred BC into the more fundamental aerosol absorption coefficient. We note that the actual BC concentration and the appropriate value for specific absorption may vary with size and the type of carbon/soot [*Clarke et al.*, 1987b].

The combination of measurements was designed to yield information on optical properties and size-resolved composition of the aerosol and its variability. With the composition and ambient humidity known the ratio of wet to dry diameter (D/D_o) or so called f(RH) [e.g., *Tang and Munkelwitz*, 1977] for the aerosol was estimated for the ambient conditions. Molar mixing rules [*Stelson*, 1990] were used to provide reasonable estimates of the effective real and complex refractive indices of the wet aerosol under ambient conditions. This information was then used as an input for Mie scattering theory in order to model the optical properties at various altitudes (absorption, scattering, and extinction coefficients of the aerosol) and to provide estimates of aerosol optical depth for comparison to values inferred from in situ measurements.

Continuous direct measurements of optical depth were made aboard the Electra using the total-direct-diffuse radiometer (TDDR). The TDDR operates by rotating a shadow arm in front of the radiometer entrance in order to measure total and diffuse irradiance; the direct solar irradiance is then obtained by subtraction [*Valero et al.*, 1989]. The data are available for seven wavelengths (380, 412, 500, 675, 862, 1064 and 1640 nm) with 10-nm bandwidth. In this fashion the TDDR characterized optical depth continuously during the descent with both an accuracy and precision better than 0.005. The differences in optical depth measured at different altitudes are related to the extinction caused by the intervening aerosol. In clear air with no clouds aloft the TDDR measures optical depth due to both aerosol extinction and Rayleigh scattering. Here we will focus upon intercomparisons of the 500-nm TDDR data (with the Rayleigh component removed) with the extinction modeled at 500 nm based upon the aerosol microphysics described above.

Observations

Column Aerosol Properties

Electra flights 8 and 9 on June 15 and 16, 1992, provided descent profiles in clear air masses but with different aerosol characteristics. A vertical profile of CN, aethaelometer-derived aerosol light absorption coefficient B_{abs}, and ambient RH are shown in Figure 1 for June 15. CN are shown corrected to STP values so that relative changes can be compared directly and regardless of altitude (pressure) changes. At all altitudes below about 3000 m the aerosol is representative of a polluted air mass with both B_{abs} values and CN concentrations well above those measured about 200 km away in "clean air" from the central Atlantic (e.g., CN about 300 cm^{-3} and BC < 50 ng/m^3, (A.D.Clarke et al., Atmospheric nuclei and related aerosol fields over the Atlantic: Clean subsiding air and continental pollution during ASTEX, submitted to *Journal of Geophysical Research*, 1995; hereafter referred to as submitted manuscript, 1995). Lowest concentrations are seen in dry air above the primary inversion located near 2000 m. The transition layer between about 400 m and 2000 m has RH near 40% and contains the most polluted air, with a peak concentration between 400m and 1000 m. In the surface layer below 400 m the RH doubles to about 80%, but CN and B_{abs} concentrations drop to about 1/3 of peak values. The near constancy of these data in this near-surface layer shows that the aerosol can be considered to be mixed up to the secondary weak inversion just below 400 m. In order to suppress short-term fluctuations caused by low signal to noise, B_{abs} has been smoothed with a 15 point Gaussian weighted running mean so that abrupt transitions are less defined than for the CN. The related BC concentrations in nanogram per cubic meter, based upon a mass absorption coefficient of 10 $m^2 g^{-1}$, can also be read directly from the B_{abs} scale (i.e., 1000 x 10^{-5} m^{-1} read as 1000 ng m^{-3}). It is clear that under these decoupled boundary layer conditions, aerosol measurements made in the surface region (e.g., ships and on land) can vary independently from the aerosol in the transition layer aloft. A more extensive discussion of aerosol properties in this air mass can be found elsewhere (A.D. Clarke et al., submitted manuscript, 1995).

Aerosol size distributions were measured during vertical profiles, but thermal scans had to be suspended for the OPC and DMA instruments due to the long time (~10 min) required for a measurement. However, thermal scans collected during nearby horizontal legs flown at selected altitudes enabled us to determine aerosol size dependent volatility characteristic of the profiled aerosol. Figure 2 is an example of a typical thermal analysis from the DMA system presented as volume distributions such that the area under the curves are proportional to aerosol volume. This example reveals that about 30% of the volume (mass) was lost at 150° C and 92% lost by 300°C, leaving a refractory residual peak at a mass mean diameter near 0.15 μm compared to the original dry diameter of about 0.3 μm. Number distributions (A.D. Clarke et al., submitted manuscript, 1995) show little reduction in concentration upon heating. This behavior and the fact that most submicrometer mass was sulfate (volatile) [*Zhuang and Huebert*, this issue] reveals that the aerosol was predominantly internally mixed with a refractory core. Similar thermal response was present in the OPC data. A comparison of the refractory mass remaining after heating with the BC data indicated that this refractory residual volume was usually between 30% and 100% BC (A.D. Clarke et al., submitted manuscript, 1995).

If we assume that the volatile mass is in the form of sulfate only, then the mean volatility in the pollution plume suggests an ammonium to sulfate ratio of about 0.7 [*Clarke*, 1991], while chemical measurements of the ratio on filter extracts suggest a value nearer 0.9 [*Zhuang and Huebert*, this issue]. Our inferred OPC sulfate mass also agreed within 20% of sulfate

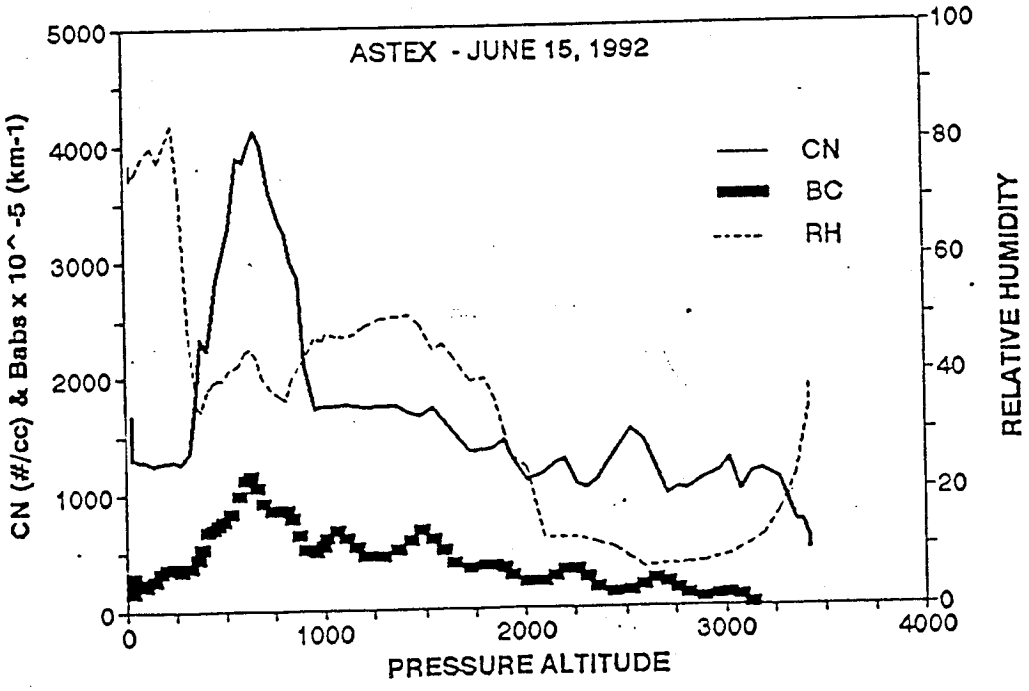

Figure 1. Vertical profiles for RH, condensation nuclei (CN), and aerosol light absorption coefficient (derived from black carbon (BC). Due to pressure effects on the aethaelometer signal during descent, B_{abs} values should be considered as illustrative and are likely to be overestimates at lower values (~100 x 10^{-5} km^{-1}).

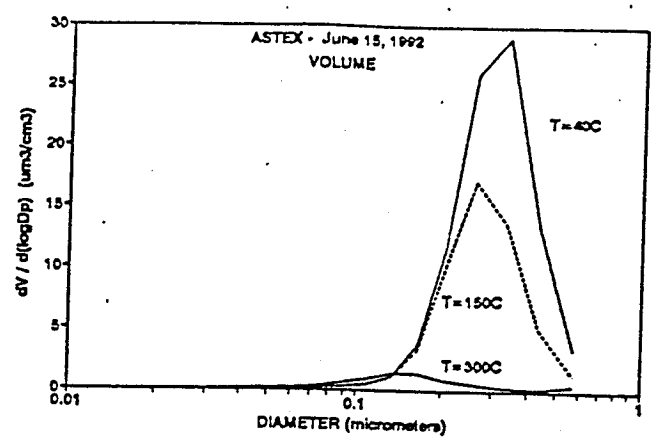

Figure 2. Example of change in volume distribution upon heating to 150° and 300°C as measured by a differential mobility analyzer. Note that the refractory residue at 300°C is shifted to smaller diameters. Although most of the mass is volatile the aerosol number (not shown) showed little change, indicating an internally mixed aerosol [*Clarke et al.*, this issue].

mass determined by these chemical measurements when averaged over extended sample legs [*Zhuang and Huebert*, this issue]. In spite of this reasonable agreement, we cannot exclude the possibility that some of the volatile mass evident at 150°C could be organics which would both lower our sulfate estimate and raise our molar ratio estimate. Because we have no information on an organic component and because it has been argued that organic particles should have similar scattering efficiencies as sulfate [*Penner et al.*, 1993], we treat the volatile fine particle dry volume as being sulfate only and use a density of 1.8 g cm^{-3} to convert it to mass. Our thermal OPC analysis [*Clarke et al.*, 1987a] has also shown that the sea-salt mass distribution is concentrated in supermicrometer sizes. Nitrate present in this pollution aerosol was also found in the coarse size range but at concentrations less that 5% of the total coarse aerosol [*Zhuang and Huebert*, this issue].

Aerosol Measurement and Optical Model

In view of the above, we have modeled the aerosol for the profile shown in Figure 1 with a fine mode composition inferred from size resolved volatility similar to that shown in Figure 2. For most of the data presented here we took 0.65 μm as the break point between dry particle fine and coarse modes. Most data in the polluted region behaved similarly to the data in Figure 2, with a slight tendency to shift to larger or smaller sizes at higher or lower concentrations, respectively. We interpret the data as representing a refractory core that contains significant BC with a diameter that is 45% of the dry aerosol diameter (ca. 10% of the mass) and coated with an acid sulfate. The water associated with the fine mode was determined from assessment of the amount of water that would be taken up by this measured dry sulfate component at the relative humidities found over the altitude range associated with a given sample (Figure 2). This has been published for ammonium bisulfate and sulfuric acid [*Tang and Munkelwitz*, 1977; called T&M hereafter]. We have measured aerosol growth in the laboratory for similar mixed salts with molar ratios over the 0.3 to 0.9 and found ratios of wet to dry diameters (D/D_o) (J.N. Porter, and A.D. Clarke, An aerosol size distribution model based on in situ measurements: Aerosol backscatter calculations, submitted to *Journal of Geophysical Research*, 1995) that lie between pure sulfuric acid and ammonium bisulfate shown by T&M and which do not exhibit an efflorescence upon drying down to 10% RH, presumably due to an excess of sulfuric acid. For example, D/D_o values at 70% RH are about 1.62(T&M) for sulfuric acid, 1.4 (T&M) for ammonium bisulfate, and 1.50 for the average of the above molar ratios. At 20% RH these values are 1.3 (T&M) for sulfuric acid, 1.0 (T&M) for ammonium bisulfate (dry), and 1.17 for our average mix. Molar mixing ratios [*Stelson*, 1990] were then used for the components and their associated refractive indices to get the effective refractive index of the aerosol mix at ambient conditions during the descent. The coarse mode was similarly modeled as a "wet" sea-salt aerosol for the June 15 "pollution" profile. The "dust" layers in the June 16 profile were modeled as a dry dust aerosol in the coarse mode. These had size-dependent corrections applied for aerosol inlet transmission losses, as previously characterized for our system aboard the Electra [*Porter et al.*, 1992].

Based upon the inferred chemistry and the "growth" described above, the ambient aerosol mixture and the corresponding refractive index were determined. We also selected the chemically measured $NH_4^+/SO_4^=$ ratio of about 0.9 [*Zhuang and Huebert*, this issue] for determination of the real component of the refractive index. Mie scattering was then applied to the resulting "ambient" size distribution in order to determine the scattering extinction due to the aerosol over selected size classes and altitude ranges. For pollution aerosol, Mie scattering was calculated based upon a spherical shell model (MIELAY) with an insoluble soot core [*Ackerman and Toon*, 1981]. The dust size distribution (Figure 8) was modeled as spherical particles with correction for transmission losses into our instruments based upon earlier Electra flights [*Porter et al.*, 1992]. Irregular dust particles are expected to scatter more than equivalent spheres [*Koepke and Hess*, 1988]. However, the size distribution upon which the model is based was collected by an OPC that should have sized dust particles larger than their equivalent sphere sizes for the same reasons. We assume here that this provides some compensation for the postulated model underestimate caused by our spherical assumption. The coarse mode was also modeled as a dust aerosol only (no soluble components) so that no growth as a function of RH was employed. The refractive indices used (real, imaginary) were as follows: ammonium/sulfate 0.9 (1.469, 9.2 x 10^{-9}), water (1.33, 2 x 10^{-9}), sea-salt (1.5, 1 x 10^{-8}), dust (1.53, 0.008), and soot (2, 0.66). The selected altitude ranges were established by the time taken to accumulate a stable aerosol distribution during descent (usually several minutes). The result of this modeling provides the contribution to optical depth for each altitude range (the differential optical depth) for which a size distribution exists. These results can then be compared to differential optical depths derived from in situ TDDR measurements aboard the aircraft.

TDDR Measurements

The in situ measurements of optical depth with the TDDR were carried out continuously during the descent profile shown in Figure 1. A time series of the TDDR measurements and altitude is shown in Figure 3 with the Rayleigh contribution to optical depth removed. Each symbol indicates a data point. Note that the values tend to alternate in sequence. This was a consequence of the data processing related to shadowband position and has been suppressed here by using a weighted running mean to smooth the data. The horizontal portion of the

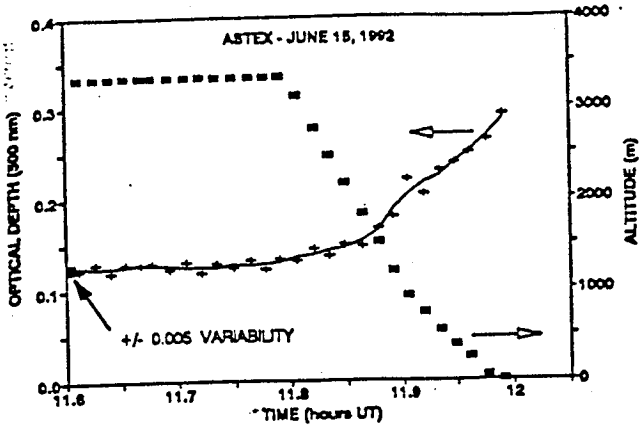

Figure 3. Altitude profile during descent and concurrent TDDR optical depth measurements for June 15. TDDR variability during a horizontal flight is taken as a measure of variability above that altitude during descent.

flight is used to estimate the range of variability in optical depth observed above aircraft altitude prior to descent. In this case the initial optical depth was about 0.125 with a variability of about ±0.005 or 4% of the total optical depth. It is assumed for the descent that this variability aloft persists during the 12-min descent and that the aerosol structure evident in Figure 1 was horizontally homogeneous. The actual change in optical depths over an altitude interval is determined from the smooth line shown in Figure 3. When divided by the altitude change, this differential optical depth is the effective extinction coefficient B_{ext}, of the aerosol over that altitude range. This can then be compared to the modeled aerosol B_{ext} over the relevant altitude ranges.

Results

June 15 Profile

Figure 4a shows the comparison of B_{ext} derived from the TDDR and modeled values based upon microphysics/chemistry for the altitude intervals over which the OPC size distributions were integrated. The horizontal arrow indicates the expected uncertainty for the TDDR B_{ext} values due to the predescent variability mentioned above. Two modeled results are shown. The solid line is for the soot-core (fine particle) and sea-salt (coarse particle) aerosol model. The dashed line is the B_{ext} that would result if the soot core were replaced by more sulfate. The effect of the soot core is seen to increase B_{ext} slightly relative to the sulfate-only case. There is a tendency for model values to be less than measured values at lower RH (above 2 km) but greater than measured in the high-RH layer at the surface. However, the integrated column differential optical depths are 0.160 +/- 0.07 for the TDDR (Figure 3) and 0.157 +/- 0.034 for the model due to the compensating effects just mentioned.

Based upon the aerosol size and inferred composition, it is possible to calculate the contribution to aerosol extinction from coarse and fine aerosol. The coarse aerosol was modeled as sea salt, and the distinction between coarse and fine for these calculations was based upon the intermode minimum present in the aerosol volume distribution that varied between about 0.6 and 0.9 μm. Figure 4b shows the modeled coarse and fine extinction for comparison to the TDDR. The only significant contribution to the coarse extinction is seen to be in the surface layer where both sea salt and high RH result in an increased contribution from larger particles. Note that the fine particle contribution to B_{ext} actually decreases for this layer from values in the layer above. This would be expected from the aerosol variability indicated in Figure 3, although the decrease is less evident in Figure 4b due to increasing near-surface extinction arising from the higher RH (Figure 1). The calculated values overpredict extinction for this layer by about 10% (Figure 4a), but it is not clear whether this is due to the uncertainties in modeling coarse or fine aerosol contributions or to a violation of the assumed horizontal homogeneity in the aerosol column "seen" by the TDDR during the descent. Horizontal legs subsequently flown adjacent to this descent showed variability over a similar time interval (say 15 min) of the order of 10-15%. In spite of this, the overall agreement between the measured and modeled optical depth suggests that the aerosol optical properties modeled from the measured microphysics are a reasonable representation of the ambient aerosol.

A recent evaluation of measurements needed to improve our assessment of anthropogenic sulfate and its radiative effects [*Penner et al.*, 1993; *Charlson et al.*, 1992, *Kiehl and*

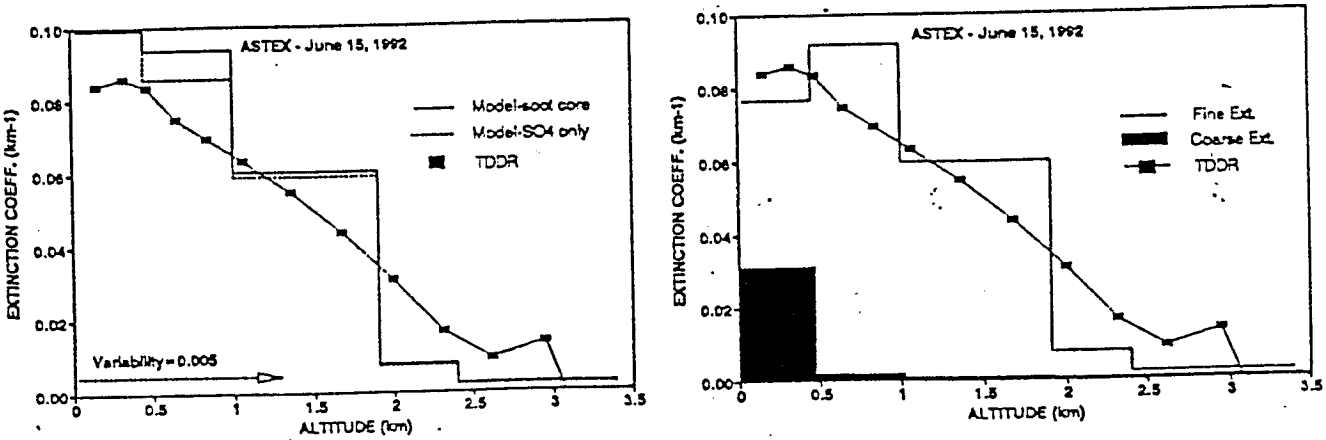

Figure 4. (a) The differential extinction coefficient from TDDR data and calculated from aerosol microphysics and chemistry (see text) for aerosol with a soot core and for equivalent diameters with sulfate composition only. (b) Extinction from soot core model separated into coarse and fine aerosol contributions.

Briegleb, 1993] have identified the scattering by the fine particle aerosol (includes all components) per mass of sulfate as a key parameter. Since this pollution plume is dominated by fine particle sulfate of european origin [*Zhuang and Huebert*, this issue], we will assume that it is representative of the typical anthropogenic aerosol discussed by these authors. Based upon the agreement between our modeled extinction and those measured by the TDDR in this plume, we also assume that our model is appropriate and that we can use it to obtain the fine particle sulfate mass scattering coefficient for this example.

Figure 5 shows the calculated ambient sulfate mass scattering coefficient for the internally mixed BC-SO_4-H_2O aerosol described above and represents the scattering coefficient, B_{sp} of the mixture divided by the inferred SO_4 concentration. High values near 16 $m^2 g^{-1}$ are evident in the humid surface layer; and low values in the dry air aloft. Volatility measurements suggested about 10% of the dry fine particle mass in the lowest surface layer to be sea salt which with associated water, contributed about 25% to the total scatter. The variations in density of the aerosol mixture are also shown at each altitude and provide an indication of the water present in the mixture. The large range (4.5-16 $m^2 g^{-1}$) for the mass scattering coefficient for sulfate encompasses the estimated average troposphere value of 8.5 $m^2 g^{-1}$ used in recent models [*Charlson et al.*, 1992].

Although the mass scattering coefficient for sulfate (defined above) may be well suited to modeling and interpreting the role of anthropogenic sulfate on radiative transfer, it is also of interest to compare the mass scattering coefficient for the total fine particle aerosol mixture (i.e. total fine scattering/total fine mass). This is shown in Figure 6 and reveals considerably less variation with height and RH. The lowest values for the dry conditions above 2 km (Figure 1) are about 3.3 $m^2 g^{-1}$. This agrees well with the average measured scattering (nephelometer at 550 nm) per dry fine particle mass reported at 3.1 ±0.2 $m^2 g^{-1}$ for five industrially influenced regions [*Waggoner et al.*, 1981] and provides further support for the validity of the approach used here. Also shown in Figure 6 is what we define as the scattering coefficient per unit volume that is derived from the ambient fine particle scattering per unit fine particle ambient volume. This shows even less variability with respect to both height and RH. It averages about 5 x 10^{-12} m^2 μm^{-3}, and its stability may be of significance. If this can be shown to be characterisitic of other pollution aerosol types,

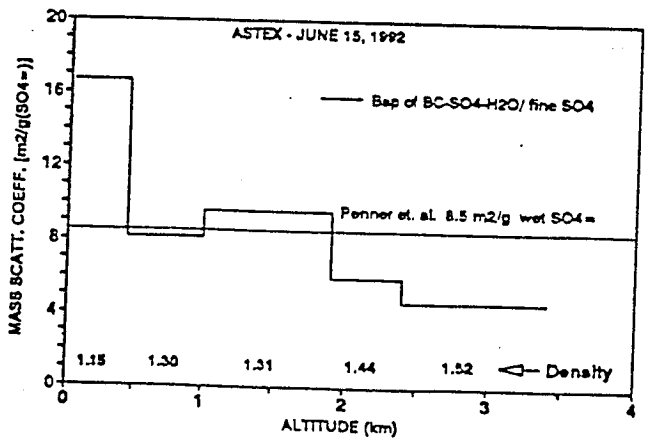

Figure 5. Calculated fine particle scattering per unit mass of sulfate for models with and without a soot core. Aerosol density shown on bottom scale as a measure of water present.

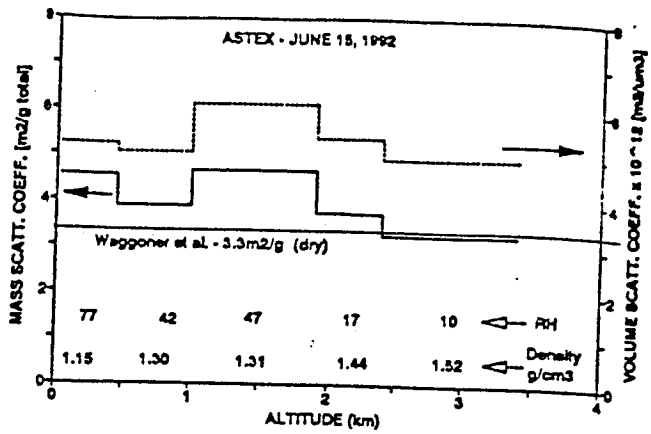

Figure 6. Scattering per unit fine particle volume and per unit fine particle total mass for aerosol.

then it may offer a simple means for converting volume distributions (regularly obtained by airborne optical particle counters) directly into extinction coefficients and column optical depths without the need to account for variations in RH or refractive index.

June 16 Profile

The previous example represented our most reliable intercomparison under the most stable aerosol conditions. However, it is of interest to compare this case with another that is also typical of this region. On the following day, June 16, 1992, the Electra completed a second clear air profile when both microphysical and TDDR measurements were available. On this day the aerosol vertical profile was more complex (Figure 7). The light absorption coefficient B_{abs} inferred from the aethaelometer and indicative of pollution was similar to values from the previous day only lower in the cloud region below 1000 m. The high CN count near 1300 m is at the top of the maximum light absorption (BC) layer rather than colocated with it, as it was on the previous day. The reason for this remains unclear. Further aloft near 2200 m the RH, CN, and B_{abs} take a sharp drop downward associated with another transition in aerosol character.

This transition is illustrated more clearly in Figure 8 where selected size distributions are plotted on the same scale for six representative altitude ranges. The near surface distributions are characteristic of the pollution aerosol present throughout most of the column on the previous day (not shown). However, at 2-km altitude the fine particle aerosol mass has decreased and continues to decrease with altitude to very low values. At the same time, the coarse particle mass increases dramatically when RH and CN drop at 2500 m, consistent with a dust plume. At this time of year, layers of Saharan dust are common both for this region and extensive areas of the North Atlantic in lower latitudes [*Schütz*, 1980; *Prospero and Carlson*, 1972]. This coarse particle dust reaches a maximum near 3 km and gradually decreases to low values near 4 km. This change in the character of the size distribution with height results in variability in most aerosol optical parameters. The small relative maximum in B_{abs} at 3 km reflects the absorption due to dust.

The TDDR data associated with this descent are shown in Figure 9. Note that on the horizontal flight leg at 3.5 km prior to descent the TDDR optical depth is much higher than on the

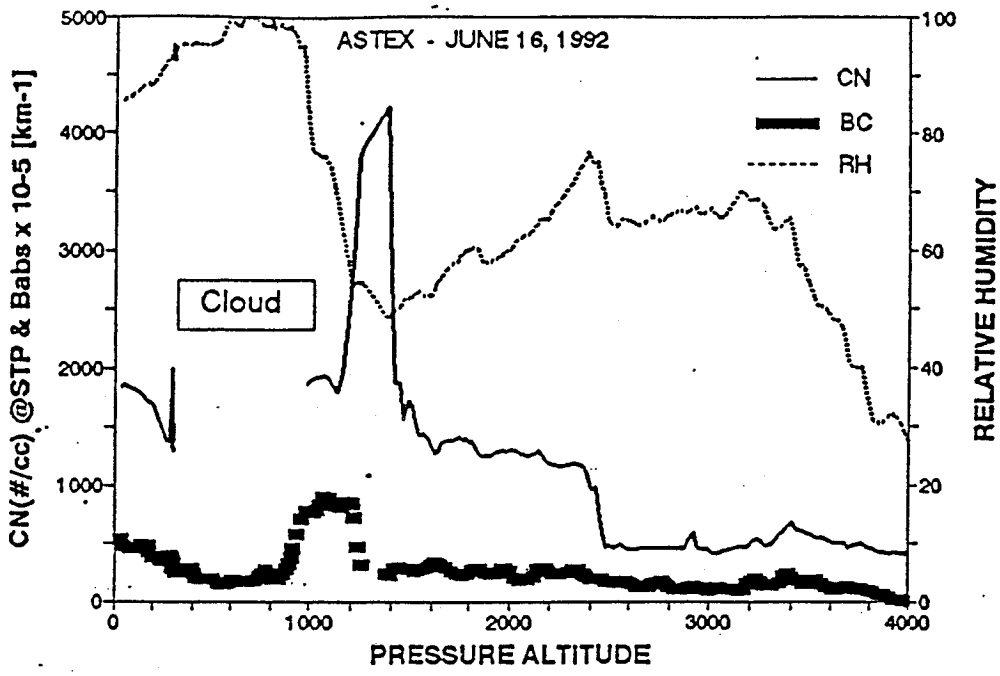

Figure 7. Same as Figure 1, only for June 16, 1992.

previous day. It also varies by ±0.03, indicating significantly greater aerosol concentration and variability above the flight altitude than for the previous day (Figure 3). The climb to 4 km immediately before descent is also associated with a slightly lower optical depth, indicating that we are already in a variable aerosol at 3.5 km that exhibits both horizontal and vertical structure. The optical depth is seen to increase substantially during the descent but, is terminated at about 1 km due to clouds.

A comparison of the measured and modeled aerosol extinction is shown in Figure 10a. The extinction determined from both methods can be seen to agree well at the beginning and end of the profile but differ substantially at middle altitudes. However, the variability in TDDR data prior to descent is seen to be about half of the observed signal (as indicated by the arrow). This variability is likely to persist during descent and may even increase as we encounter more optically thick layers. We expect that this variable aerosol column above the aircraft contributes significantly to the disparity between measured and modeled extinction at middle altitudes, since the TDDR responds to changes in concentration throughout the column while the modeled behavior is based on in situ data at the aircraft altitude. Clearly, a remote sensing capability such as an onboard lidar is needed to resolve such uncertainties. Nevertheless, we cannot discount model limitations due to the possibility of poorly characterized dust size distributions, incomplete corrections for sample losses, errors in refractive indices or the role of nonsphericity in the model results.

The separate coarse and fine particle modeled extinction is shown in Figure 10b and clearly reveals the difference in aerosol type above and below the 2-km inversion. Above the inversion the extinction and optical depth are dominated by the coarse particle dust, while below it they are dominated by the fine particle pollution aerosol similar in physical and chemical properties to that observed on the previous flight and discussed earlier. The contributions of coarse and fine aerosol to the modeled column extinction at 1 km are roughly equal for this case. Aerosol layering like this and the occasional depletion of near-surface aerosol seen on ASTEX emphasizes that surface aerosol measurements may not represent column aerosol concentrations (see Figures 1 and 2), since they may not characterize a major aerosol type that is contributing to column optical depth.

Discussion

In any attempt at closure, intrinsic uncertainties exist that are related to uncertainties in the effective size and refractive index of the modeled aerosol. Here we are attempting to assess closure beteen the calculated extinction based upon size-resolved physicochemistry and extinction measured directly during descents through variable aerosol fields. Uncertainties are primarily due to the size calibration uncertainty in the OPC, the inferred composition, aerosol growth, uncertainty in measured average RH over a sample period, and TDDR uncertainty. The effects of these uncertainties are estimated in Table 1 for a nominal fine sulfate distribution and coarse sea-salt distribution similar to those observed. We are interested in sensitivity of the calculated scattering coefficient for the distribution to changes in individual parameters. Hence we show the calculated percentage change in scattering for a 1% change in parameter values while holding all other parameters constant. Next we give our best estimate of expected uncertainties in these parameter values for the data discussed here. The product of these two numbers is shown and gives the expected uncertainty in the integral scattering due to each of these parameters, assuming that the variations are independent. By this we mean that even though a change in RH will affect scattering both through a change $f(RH)$ and R_e this is distinct from the uncertainty in selecting the proper $f(RH)$ for a given RH and composition. Uncertainties in $f(RH)$ are based upon scatter about our calibration data mentioned above for mixtures of ammonium to sulfate ratios between 0.3 and 0.9. The OPC

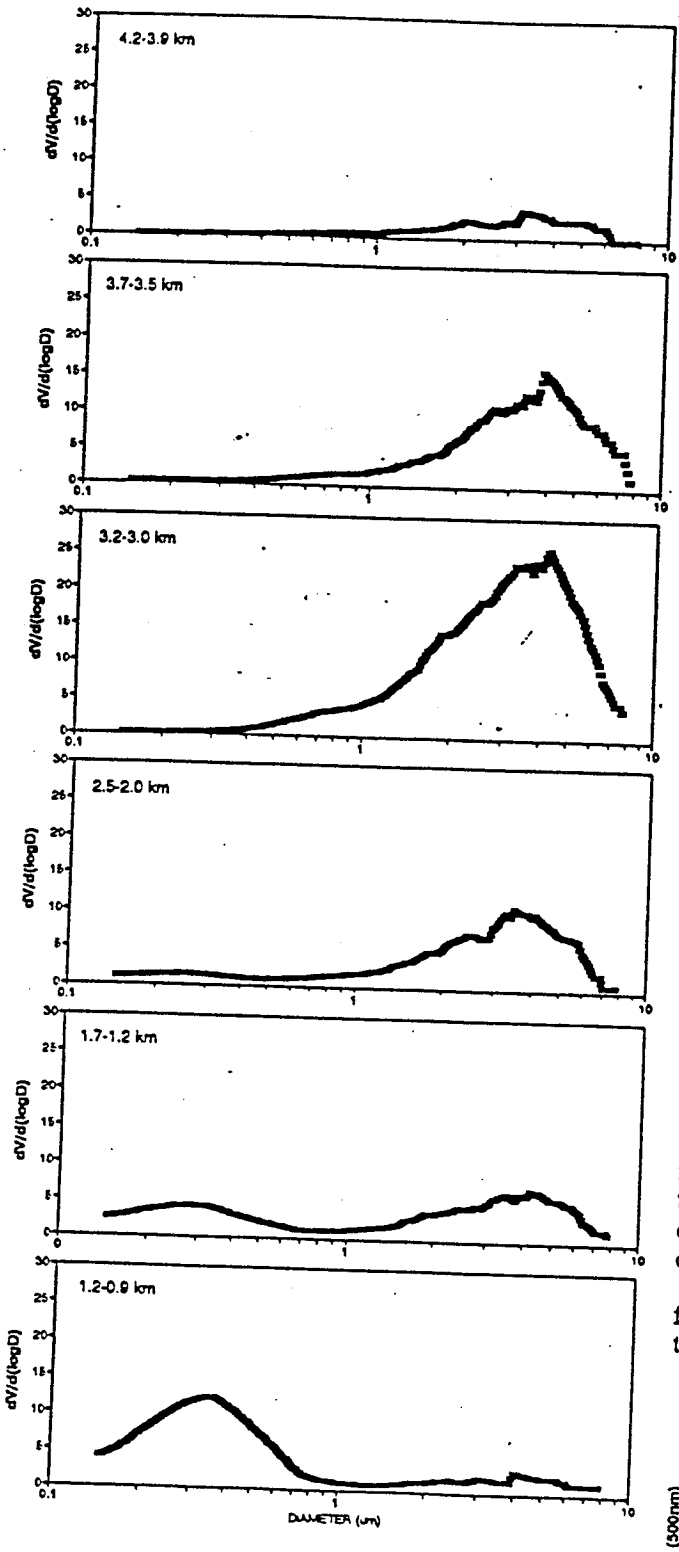

Figure 8. Aerosol volume distributions from the OPC for the descent profile shown in Figure 7. Note dominance of fine particle aerosol near surface and coarse aloft.

D_p uncertainty is based upon our uncertainty in calibration for the OPC during field use. This has been introduced into a typical lognormal distribution mass mean diameter for calculating resultant scattering uncertainty for the distribution.

A similar procedure was used for the spread parameter of the distribution, sigma, RH, refractive index (R_e), etc. The uncertainty in measured RH change when going from OPC RH to ambient is estimated at about 5% based upon our experience in using RH sensors (Vaisala nominally ±2%RH) under field conditions and with recent calibrations. The uncertainty in R_e is based upon our expectation that our ammonium sulfate ratio is accurate to about ±0.1 and that water is dominating the volume at 70%RH. For the coarse sea-salt aerosol it is based on the assumption that NaCl and water are the only constituents. These contributions are then combined as the square root of the sum of the squares of these uncertainties to get the overall uncertainty for each of the indicated fine and coarse distributions. The actual results shown elsewhere in this paper are based upon measured OPC distributions rather than a lognormal as illustrated in Table 1 but because the OPC distribution is generally well described by lognormal fits to coarse and fine modes, the indicated uncertainties are expected to be similar.

Because the scattering cross section is such a strong function of particle size for the smaller aerosol discussed here, the uncertainties in resultant scattering tend to be greater for the sulfate case than for the coarse sea salt (Table 1) or dust (not shown in Table 1) in spite of greater sizing uncertainties for the coarse aerosol. On the other hand, although inlet loss corrections have been applied for the larger aerosol, there may be uncharacterized losses for the largest sea-salt and dust aerosol. However, these will be less significant for the scattering/extinction than for aerosol mass because of the low scattering per unit mass of the larger aerosol.

The TDDR uncertainties in optical depth are less than 0.005 in both precision and accuracy (F. Valero, unpublished data, 1995) and are less of a concern for the above comparisons to in situ data than the effect of atmospheric inhomogeneities on the optical path seen by the TDDR. In the two cases shown for June 15 and 16 the latter were estimated as variability in optical depth prior to descent of 0.005 and 0.03 respectively over distances comparable to that covered during the descent. These correspond to 4% and 17%, respectively, of the optical depths at those altitudes. If this variability persists (or possibly increases) within the TDDR view path during descent through the aerosol column, then this variability will result in a disagreement between TDDR and in situ measurements that could exceed the uncertainty in the measurements themselves.

The disagreement between TTDR and in-situ data evident for the higher altitudes during the June 16 descent is due in part to this problem. Evidence for this can be seen in Figure 9.

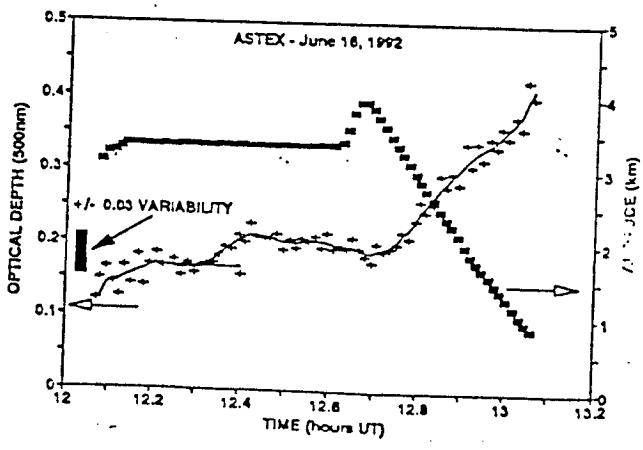

Figure 9. Same as Figure 3, only for June 16.

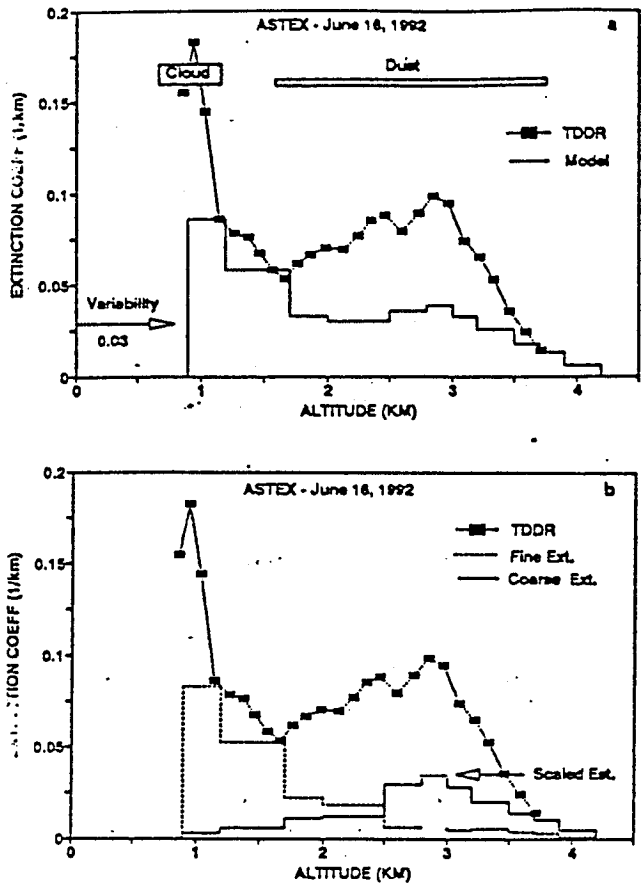

Figure 10. Same as Figure 4, only for June 16 and including dust aloft.

Based upon the general agreement seen in Figure 4 we consider the fine particle contribution to extinction reasonably well modeled. Hence the modeled fine particle contribution shown in Figure 10b can be subtracted from the measured TDDR extinction at each altitude to leave the effective TDDR coarse particle extinction. This can be compared to the modeled value over each OPC altitude range. Since the measured dust distribution shown in Figure 8 changes only in amplitude and not in shape we expect that any systematic difference between measured and modeled dust extinction should be reflected as a constant ratio. However, near 3.5 km this ratio is about one while between 2 and 3km it is greater than 2. We interpret this change in the ratio of modeled to measured dust optical depth to be caused by horizontal inhomogeneities in the aerosol "seen" by the TDDR during the descent.

In spite of these limitations, the data presented above allow some comparison of properties of dust and pollution aerosol after transport to the marine environment. Clearly, both aerosol types are important to column optical properties, and both can occur simultaneously in the atmospheric column. The data also demonstrate the importance of water uptake by aerosol to their optical properties. The influence of the latter is clear from Figure 5 where the scattering coefficient per sulfate mass is elevated in the near-surface layer due to high RH. When expressed as scattering per unit total mass (Figure 5b) the influence of changing composition with RH is much smaller. This is in part due to the fact that the size-dependent mass scattering coefficients for ammonium sulfate (dry) and for water are very similar in shape and peak value (~ 6 $m^2 g^{-1}$). The former reaches its maximum value near 0.5 μm and the latter near 0.8 μm [*Ouimette and Flagan*, 1982]. Hence growth of the dry distribution (mass mean D_p=0.3 μm)modeled here (Figure 2) can have similar values in both the dry and highly hydrated states. As the mass increases, the refractive index drops, but the scattering cross section inereases such that the scattering per unit mass changes only slowly, becoming somewhat higher at higher RH. Because density also decreases as RH is increased (Figure 5) this parameter shows even less variability with altitude (RH) when expressed as scattering per unit volume (Figure 5b).

The influence of internally mixed soot on extinction was shown to be small except under higher pollution cases and dryer conditions, where it contributed about 10%, as seen in Figure 4. Modeled internal and external mixtures of soot and sulfate resulted in negligible difference in total extinction (not shown), although the absorption component increased slightly for soot mixed internally as soot cores, while the scattering component increased for externally mixed soot.

The composition also affects the single scatter albedo (SSA), another fundamental aerosol parameter required for modeling aerosol optical properties. This is the ratio of the aerosol scattering coefficient to the sum of both scattering and absorption coefficients (total extinction). At visible wavelengths, pure salts and water have SSA values approaching 1. As soot is added the SSA decreases, and values as low as 0.7 have been observed in remote marine environments influenced by combustion sources [*Clarke*,

Table 1. Uncertainty Estimates for Modeled Aerosol Parameters

	Sulfate, D_p=0.24 μm, Sigma=1.24					NaCl, D_p=3.0 μm, Sigma=1.5				
	D/D_o	OPC D_p	Sigma	RH	R_r	D/D_o	OPC D_p	Sigma	RH	R_r
After growth at 70%RH										
% Scatter / % parameter	3	1.5	1.8	2.2	3	3	0.9	0.2	1.1	<0.1
Parameter uncertainty, %	4	5	5	5	1	2	10	10	5	<10
Scatter uncertainty, %	12	15	7.5	9	2.2	6	9	2	5.5	< 1
Sqrt-Sum-Sq, %	22					12				

R_r, refractive index; Sqrt-Sum-Sq, square root of the sum of the squared uncertainties.

1989]. However, as water is added the relative effect of the soot is reduced, and SSA values increase. All of these effects can be seen in the SSA values plotted in Figure 11 for the two profiles. Here we have taken the calculated scattering coefficients based on the size distribution and added the absorption coefficient obtained from the aethaelometer to get the total extinction. The June 15 pollution profile has high SSA values near the surface due to the relative influence of the water uptake, but low values aloft due to the influence of soot. The June 16 profile has similar SSA values in the pollution layer at 1-2 km, but higher values aloft in the peak dust layer near 3 km. We have also indicated the SSA values for calculated scattering and extinction for June 15 from comparison to SSA derived from measured B_{abs}. The trends in SSA are the same but values are lower in the more polluted layers and higher aloft for the calculated values. If the relative composition of the dry aerosol is constant, as presumed in the model, this suggests that possibly the humidity measurements may be in error or the presumed growth in the lower layers may be too large, and in the upper layers too small.

The size-resolved characterization of the dust plume on June 16 also allows an estimate of its optical properties. If we use a density of 2.5 g m^{-2} for dust and the integral volume distribution at 3.0-3.2 km (Figure 8) we get a mass concentration of about 35 μg m^{-3}. Dividing the value for B_{abs} (Figure 7) of about 200 x 10^{-5} m^{-1} at 3 km by this mass concentration yields a mass absorption coefficient for the dust of about 0.06 ± 0.015 m^2 g^{-1}. We assume that the modeled extinction is possibly an underestimate of the real values, while the TDDR values are probably an overestimate for reasons mentioned earlier (Figure 10b). In view of this, we use an extinction value at 3 km of 0.04 ± 0.01 km^{-1} and the same mass concentration to get the mass scattering coefficient for the dust of 1.1±0.2 m^2 g^{-1}. This value for dust is lower than the value of 3.2 to 4.7 m^2 g^{-1} found for the pollution plume that was dominated by extinction due to fine particle sulfate. It is also higher by a factor of 3 when compared to values for earlier aircraft data obtained in dust layers near Cape Verde Islands and closer to the Sahara source region [*Carlson and Caverly*, 1977] but much closer to their values of 1.25-1.7 m^2 g^{-1} measured 4000 km further downwind at Barbados. For aged dust, higher values are to be expected further downwind, since the larger particles have been depleted due to their more rapid sedimentation [Schütz, 1980]. This is because larger particles with the highest mass are less efficient scatterers on a mass basis. Because the trajectory for our dust layers first went north over southern Europe before swinging west to the Azores (C. Bretherton, personal communication, 1994), our values for extinction per unit mass are consistent with our intermediate trajectory distance.

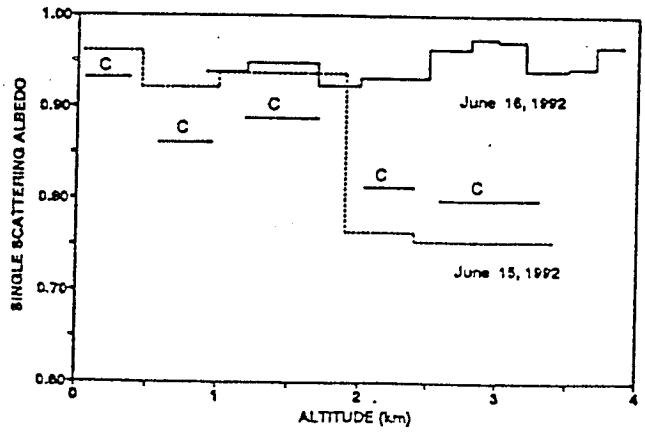

Figure 11. Aerosol single scatter albedo for both flights as obtained from the calculated scattering coefficient and the aethaelometer derived B_{abs}. Model calculated values (C) also shown for comparison.

Conclusions

We have presented vertically resolved column measurements of aerosol physicochemistry and related optical properties with the objective of testing aerosol radiative closure in the perturbed marine atmosphere over the Atlantic. Two flights that included continental pollution and Saharan dust were discussed that demonstrated the relative importance of soot, dusts, sulfate and water in the determination of atmospheric aerosol radiative properties. For the polluted case, closure was achieved within the estimated measurement uncertainties of about ±22%, indicating that existing techniques may be adequate to quantify issues related to the radiative effects of sulfate and pollutant aerosol. Reduction in measurement uncertainty will require improved assessment of aerosol growth, $f(RH)$ for ambient aerosol, careful size calibration and accurate measurement of relative humidity. The state of mixing (internal versus external) and the optical influence of the soot component appeared to have less of an impact on uncertainties in this moist marine environment.

For the dust case, the difference between modeled and measured values was considerably greater than estimated ideal measurement uncertainties (12%). Much of this difference is ascribed to the more complex variability in the vertical and horizontal dust field that impacted the light path of the TDDR measurements but not the corresponding in situ particle data. Although coarse particle measurement uncertainties can be reduced, a significant reduction in this kind of disagreement (i.e., improving column closure) will only be possible with remote sensing techniques (e.g., lidar) that continuously monitor the structure of the aerosol field that affects the optical measurement. In spite of these uncertainties, the data demonstrate that contributions to column optical depth from dust and pollution can coexist and can be comparable.

Except for drier air (~ 40% RH), the effect of soot on extinction and single scatter albedo was generally only a few percent and generally far less than the effect of water, particularly when integrated over the aerosol column. The ratio of total fine scattering to fine sulfate mass in polluted air ranged from 5 to16 m^2 g^{-1} primarily due to the effect of water uptake, but a frequently quoted mean column value of 8.5 m^2 g^{-1} [*Penner et al.*, 1993] was also representative of this case. The more physically meaningful ratio of total fine scattering to total fine mass was more stable at 4.0 +/- 0.7 m^2 g^{-1}. In drier layers aloft this value agreed with the mean value of 3.3 m^2 g^{-1} often found in polluted continental dry air [*Waggoner et al.*, 1981] and demonstrating the consistency of our data. An alternate parameter defined as the ratio of total fine scatter to total fine volume appears to be even less variable and may be convenient for the direct conversion of in situ volume measurements frequently available from aircraft into aerosol scattering-extinction data.

The internal mixing of soot and sulfate evident for this pollution plume is also of significance. While the increase in column B_{ext} due to BC was not large for this case, it could be greater in other cases. Since the sulfate and BC are often

derived from the same combustion source, both should be considered together in assessing and parameterizing the radiative effects of anthropogenic emissions.

The aerosol vertical structure in both examples was complex. While sea-salt concentrations were higher at the surface, the non-sea-salt aerosol concentrations at the surface were lower than concentrations aloft presumably due to more efficient scavenging in the boundary layer. Dust layers were also decoupled from the surface. This variability will complicate the interpretation of surface data sets that are used to infer column aerosol properties. It is also clear that other column closure comparisons of this type could reduce uncertainties appreciably by including concurrent measurement of the structure of the aerosol field (e.g., lidar) during descent profiles.

Acknowledgments. Special appreciation is extended to Barry Huebert for facilitating our activities under ASTEX/MAGE and to the management of the National Center for Atmospheric Research Aviation Facility and to the crew of the Electra for their cooperation in making these measurements possible. We thank Warren Wiscombe for the modified MIELAY codes used and Xinli Li for computer analysis. This work is a contribution of the International Global Atmospheric Chemistry (IGAC) Core project of the International Geosphere-Biosphere Programme (IGBP) and was supported through the Office of Naval Research under contract ONR N00014-92-J-1388 and by NASA under contract NAG8-848. SOEST contribution 3947.

References

Ackerman, T.P., and O.B. Toon, Absorption of visible radiation in atmospheres containing mixtures of absorbing and non-absorbing particles, *Appl. Opt.*, *20*, 3661-3667, 1981.

Ayers, G.P., and J. L. Gras, Seasonal Relationships between cloud condensations nuclei and aerosol methane sulfonate in marine air, *Nature*, 834-835, 1991.

Carlson, T.N. and R.S. Caverly, Radiative characteristics of Saharan dust at solar wavelengths, *J. Geophys. Res.*, *82*, 3141-3152, 1977.

Charlson, R. J., J. E. Lovelock, M. O. Andreae, S. G. Warren, Oceanic phytoplankton, atmospheric sulfur, cloud albedo and climate, *Nature*, *326*, 655, 1987.

Charlson, R.J., S.E. Schwartz, J.M. Hales, R.D. Cess, J.A. Coakley Jr., J.E. Hansen, and D.J. Hofmann, Climate forcing by anthropogenic aerosols, *Science*, *255*, 423-430, 1992.

Clarke, A.D., Aerosol physical chemistry in remote marine regions, *J. Aerosol Sci.*, *19*, 1195, 1988.

Clarke, A.D., Aerosol light absorption by soot in remote environments, *Aerosol Sci. Technol.*, *10*, 161-171, 1989.

Clarke .D., A thermo-optic technique for in situ analysis of size resolved aerosol physicochemistry, *Atmos. Environ. 25A*, 635-644, 1991.

Clarke, A. D., N. C. Ahlquist and D. S. Covert, The Pacific marine aerosol: Evidence for natural acid sulfates, *J. Geophys. Res.*, *92*, (D4), 4179, 1987a.

Clarke, A.D., K.J. Noone, J. Heintzenberg, S.G. Warren, and D.S. Covert, Aerosol light absorption measurement techniques: Analysis and intercomparisons, *Atmos. Environ.*, *21*, 1455-1465, 1987b.

Clarke, A.D., T. Uehara and J. Porter, Lagrangian evolution of an aerosol column during Atlantic Stratocumulus Transition Experiment, *J. Geophys. Res.*, this issue.

d'Almeida, G.A., On the variability of desert aerosol radiative characteristics, *J. Geophys. Res.*, *92*, 3017-3026, 1987.

Gundel, L.A., R.L. Dod, H. Rosen, and T. Novokov, The relationship between optical attenuation and black carbon for ambient and source particles, *Sci. Total Environ.*, *36*, 197-202, 1984.

Hooker, S.B., and E.F. Firestone, An overview of SeaWiFS and ocean color, *NASA Tech. Memo.*, *104566*, vol. 1, 1993.

Huebert, B.J., S.G. Howell, P.Laj, J.E. Johnson, T.S. Bates, P.K. Quinn, S.A. Yvon, E.S. Saltzman, V. Yegorov, A.D. Clarke, and J.N. Porter, Observations of the atmospheric sulfur cycle on SAGA-3, *J. Geophys. Res.*, *98*, 16,985-16,996, 1993.

Huebert, B.J., A. Pzenny and B. Bloomquist, The Atlantic Stratocumulous Transition Experiment/Marine Aerosol and Gas Exchange, *J. Geophys. Res.*, this issue.

Kiehl, J.T., and B.P. Briegleb, The relative roles of sulfate aerosol and greenhouse gases in climate forcing, *Science*, *260*, 311-314, 1993.

Koepke, P., and M. Hess, Scattering functions from tropospheric aerosols: The effects of non-spherical particles, *Appl. Opt.*, *27*, 2422-2430, 1988.

Ouimette, J.R. and R.C. Flagan, The extinction coefficient of multicomponent aerosols, *Atmos. Environ.*, *16*, 2405-2519, 1982.

Penner, J.E., R.J. Charlson, J.M. Hales, N. Laulainen, R. Leifer, T. Novakov, J. Orgen, L.F. Radke, S.E. Schwartz and L.Travis, Quantifying and minimizing uncertainty of climate forcing by anthropogenic aerosols, *Rep. DOE/NBB-0092T*, Dep. of Energy, Washington, D.C., March 1993.

Porter, J.N., A.D. Clarke, G. Ferry, and R.F. Pueschel, Aircraft studies of size-dependent aerosol sampling through inlets., *J. Geophys. Res.*, *97*, 3815-3824, 1992

Prospero, J.M. and T.N. Carlson, Vertical and areal distribution of Saharan dust over the western equatorial Atlantic, *J. Geophys. Res.*, *77*, 5255-5265, 1972.

Saltzman, E.S., D.L. Savoie,, J.M. Prospero, and R.G. Zika, Methanesulfonic acid and non-sea-salt sulfate in Pacific air: regional and seasonal variations, *J. Atmos. Chem.*, *4*, 227-240, 1986.

Savoie, D.L. and J. M. Prospero, Particle size distribution of nitrate and sulfate in the marine atmosphere, *Geophys. Res. Lett.*, *9*, 1207-1210, 1982.

Schütz, L., Long range transport of desert dust with special emphasis on the Sahara, Aerosol: Anthropogenic and Natural Sources and Transport, *Ann. N.Y. Acad. Sci.*, 336, 515-532, 1980.

Stelson, A.W., Urban aerosol refractive index prediction by partial molar fraction approach, *Environ. Sci. Technol.*, *26*, 1676-1679, 1990.

Tang, I. and H.R. Munkelwitz, Aerosol growth studies, III, Ammonium bisulfate aerosols in a moist atmosphere, *J. Aerosol. Sci.*, *8*, 321-330, 1977.

Twomey, S., Atmospheric Aerosols, 289pp., New York, Elsevier, 1977.

Valero, F.P.J., T.P. Ackerman, and W.J.Y. Gore, The effects of Arctic haze as determined from radiometric measurements during AGASP II, *J. Atmos. Chem.*, *9*, 225-244, 1989.

Waggoner, A.P., R.E. Weiss, N.C. Ahlquist, D.S. Covert, S. Will, and R.J. Charlson, Optical characteristics of atmospheric aerosols, *Atmos. Environ.*, *15*, 1891-1909, 1981.

Woodcock, A.H., Salt nuclei in marine air as a function of altitude and wind force, *J. Meteorol.*, *10*, 362-371, 1953.

Zhuang, L., and B.J. Huebert, A Lagrangian analysis of the total ammonia budget during the Atlantic Stratocumulus Transition Experiment / Marine Aerosol and Gas Experiment, *J. Geophys. Res.*, this issue.

A.D. Clarke and J. N. Porter, School of Ocean and Earth Science and Technology, University of Hawaii, Honolulu, HI 96822. (e-mail: tclarke@soest.hawaii.edu; porter@soest.hawaii.edu)

P. Pilewskie, NASA, Ames Research Center, Moffett Field, CA 94035. (e-mail: pil@ra.arc.nasa.gov)

F.P.J. Valero, California Space Institute, University of California, San Diego, La Jolla, CA 92093. (e-mail: fvalero@ucsd.edu)

(Received August 3, 1994; revised October 12, 1995; accepted October 12, 1995.)

REPORT DOCUMENTATION PAGE

Form Approved
OMB No. 0704-0188

1. AGENCY USE ONLY (Leave blank)	2. REPORT DATE	3. REPORT TYPE AND DATES COVERED
	10/30/96	Final Report 05/01/94-04/30/96

4. TITLE AND SUBTITLE

Radiative Effects of Aerosols

5. FUNDING NUMBERS

NAG2934

6. AUTHOR(S)

Dr. Francisco P.J. Valero

7. PERFORMING ORGANIZATION NAME(S) AND ADDRESS(ES)

University of California at San Diego
Scripps Institution of Oceanography
9500 Gilman Drive
La Jolla, CA 92093-0242

8. PERFORMING ORGANIZATION REPORT NUMBER

9. SPONSORING/MONITORING AGENCY NAME(S) AND ADDRESS(ES)

NASA
Ames Research Center
Moffett Field, CA 94035-1000

10. SPONSORING/MONITORING AGENCY REPORT NUMBER

11. SUPPLEMENTARY NOTES

12a. DISTRIBUTION/AVAILABILITY STATEMENT

12b. DISTRIBUTION CODE

13. ABSTRACT (Maximum 200 words)

(see attached)

14. SUBJECT TERMS

15. NUMBER OF PAGES
13

16. PRICE CODE

17. SECURITY CLASSIFICATION OF REPORT	18. SECURITY CLASSIFICATION OF THIS PAGE	19. SECURITY CLASSIFICATION OF ABSTRACT	20. LIMITATION OF ABSTRACT